*Bangladesh Journal of Physics, Vol. **29**, Issue 1, pp. 25 – 38, June 2022*

HIGH-FREQUENCY RESPONSE OF COMPLEX INITIAL PERMEABILITY OF Cr SUBSTITUTED $Co_{0.5}Cu_{0.5}Fe_{2-x}Cr_xO_4$

M. H. R. KHAN[1*] AND A. K. M. AKTHER HOSSAIN[2]

[1]*Department of Arts and Sciences, Ahsanullah University of Science and Technology, Dhaka-1208, Bangladesh*
[2]*Department of Physics, Bangladesh University of Engineering and Technology, Dhaka-1000, Bangladesh*

**Corresponding author e-mail: hamid.as@aust.edu*
Received on 14.03.2022, Revised received on 18.05.2022, Accepted for publication on 20.06.2022

DOI: https://doi.org/10.3126/bjphy.v29i1.78688

ABSTRACT

The Lattice parameter, density, initial permeability, saturation magnetization, and Néel temperature of the Cr substituted various $Co_{0.5}Cu_{0.5}Fe_{2-x}Cr_xO_4$ have been invented. It also explores how the sintering temperature affects these samples' density, porosity, grain size, and initial permeability. As the Cr content increases, the lattice parameter, density, and saturation magnetization decrease. The variation of lattice parameters, density, and maximum magnetic saturation level can be explained in the light of ionic size, atomic mass, and magnetic moment of Cr ion, respectively. However, grain size, complex initial permeability, and coercivity rise until x=0.2 and fall as the Cr concentration increases. Grain size, initial permeability, and coercivity correlated to each other. The textured structure of this ferrite was found at 1373K, confirmed by XRD and microstructural analysis.

Keywords: *Co-Cu ferrites, Saturation magnetization, Complex initial permeability, XRD, Néel temperature*

1. INTRODUCTION

Co-Cu ferrites are of increasing interest to researchers due to their remarkable electromagnetic properties, high Curie temperature, moderate sintering temperature, high-frequency response complex initial permeability ($\mu_i^{/}$), effective saturation magnetization (M_S), high coercivity (H_C), low eddy current loss and distinct technological requirements [1-5]. Copper-based ferrites are an important material for applications at multilayer chip inductors at low temperatures [4]. Ferrite, mixtures of iron oxides, and divalent metal oxides have spinel structures with nominal formula MFe_2O_4, where M= Co, Ni, Cu, etc. In the spinel structure, Oxygen ions are filled with tetrahedral sites called A-sites and octahedral sites called B-sites, which occupy different kinds of A^{2+} (Co, Cu) and B^{3+} (Fe, Cr) cations. In the spinel ferrite materials, a super-exchange (A-B) interaction happens between A and B cations through the oxygen. Weakening and strengthening of A-B interactions depends on how the cations are distributed between the A-site and B-site. [2]. A-B interactions and site preferences of metal ions play a significant role in various magnetic, electrical, structural, morphological, and chemical properties [6-10]. It can be seen that in inverse spinel cobalt ferrite ($CoFe_2O_4$), cobalt ions are located in the B-site, and iron ions are located in the A- and B-sites. According to S.T. Alone *et al.* [5], non-magnetic Zn favors the A-site, while Cr favors the B-site in cobalt ferrite. Ravinder *et al.* described the conductivity (electrical) of Cu-Cr ferrite as dependent on temperature and composition [9]. The magnetic and electrical properties of $Co_{0.5}Cu_{0.5}Fe_{2-x}Cr_xO_4$ ferrite are changed by substituting Cr ions due to grain size (D), M_S, and H_C dependence. However,

there are no comprehensive surveys of the morphological and magnetic features of Chromium substituted $Co_{0.5}Cu_{0.5}Fe_{2-x}Cr_xO_4$ in the literature. We want to investigate how the structure, frequency-dependent real component of M_S, Néel Temperature (T_N), and quality factor (Q) of $Co_{0.5}Cu_{0.5}Fe_{2-x}Cr_xO_4$ are affected by Cr substitution.

2. EXPERIMENTS

In the present work, ferrites with the nominal chemical formula $Co_{0.5}Cu_{0.5}Fe_{2-x}Cr_xO_4$ different samples from x = 0.0 to x= 0.4 in steps of dx = 0.1 were fabricated by the standard solid-state reaction technique. Stoichiometric amounts of basic materials $CaCO_3$, CuO, Cr_2O_3, and Fe_2O_3 each of purity 99.99%, were mixed and ground to prepare the selected samples. These were then calcined at 1100K for 5 hours in air. Toroid-shaped and disc-shaped samples were prepared. The XRD, Optical Microscope, Wayne Kerr Impedance Analyzer (model no. 6500B), SQUID Magnetometer were used to characterize the phase composition, microstructure, both frequency response and temperature dependent permeability, and M_S of every sample that was sintered at a variety of temperatures, respectively. The μ_i' over the frequency range of 100 – 120 MHz was observed. The relative quality factor (Q) is computed from the imaginary part of permeability. Each sample's M-H loops were measured at 300 and 10 K after being sintered at 1373 K.

3. RESULTS AND DISCUSSION

3.1 Structure of $Co_{0.5}Cu_{0.5}Fe_{2-x}Cr_xO_4$

The Fig.1. represents the XRD shapes of Cr-doped $Co_{0.5}Cu_{0.5}Fe_{2-x}Cr_xO_4$ samples. The reflection peaks are observed from the indexed (111), (220), (311), (222), (400), (422), (511), and (440) planes. It can be seen from the Fig. 1 that no significant secondary peaks originate in the XRD shape. The XRD shapes' peak locations verify that the samples' ferrimagnetic cubic spinel structure exists [1].

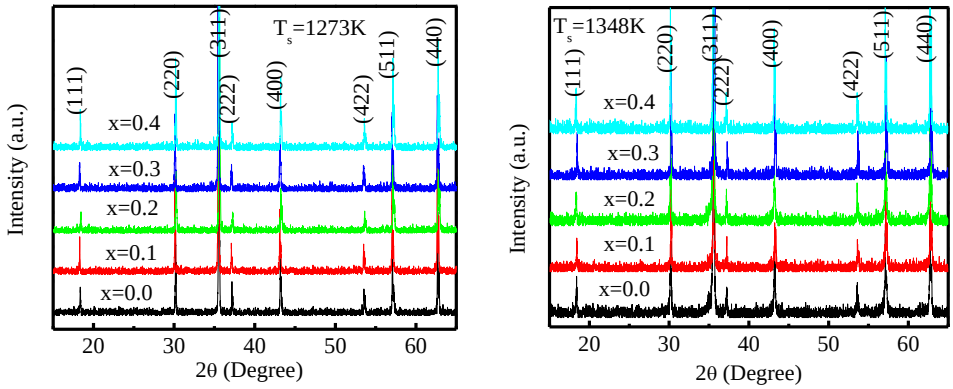

Fig. 1. XRD patterns for various $Co_{0.5}Cu_{0.5}Fe_{2-x}Cr_xO_4$ sintered at (a) 1273K and (b) 1348 K.

At higher sintering temperatures 1373K and 1473K, the samples of these compositions prefer to grow different orientations which is shown in Fig. 2. There is no XRD peak in its spectrum sintered at 1473K except only (220), (311), (400) and (440) peaks for x=0.0, (111), (311), (400) and (511) peaks for x=0.1 and (220) and (311) peaks for x=0.2. This preferred orientation ensures that the samples have textured structure [10]. No preferred orientation was found for higher contents of Cr

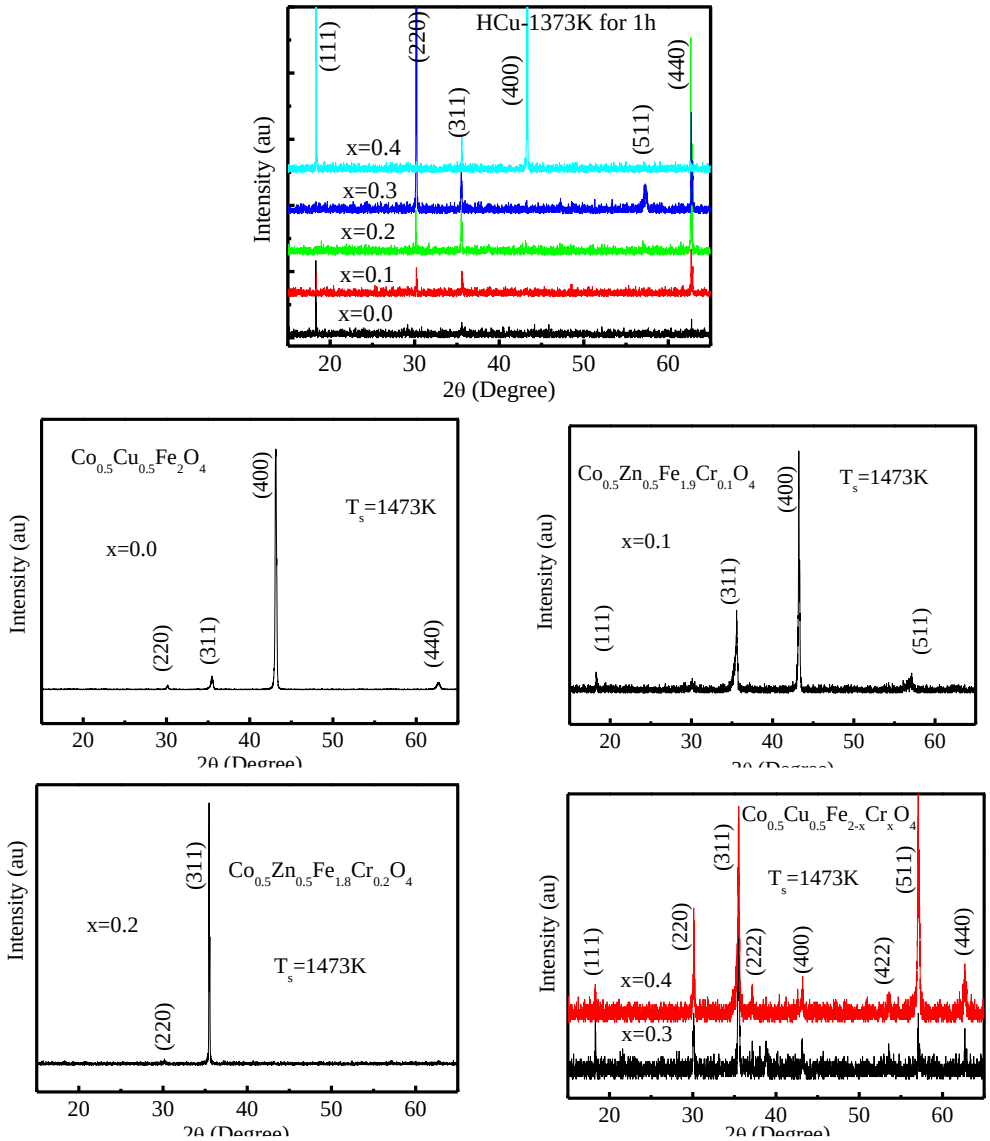

Fig. 2. XRD patterns for various $Co_{0.5}Cu_{0.5}Fe_{2-x}Cr_xO_4$ sintered at 1373 and 1473 K

at this T_s. When the T_s is increased above 1473K all indexed peaks have been seen clearly which suggests that the texture may have deteriorated. Fig. 3 shows the lattice parameter '*a*' of $Co_{0.5}Cu_{0.5}Fe_{2-x}Cr_xO_4$ with Cr concentration. As the amount of Cr increases, the '*a*' decrease from 0.8389 nm to 0.8378 nm. This happens because Cr has a smaller ionic radius (0.063 nm) than Fe (0.67 nm). No noticeable difference of '*a*' is visible between sintered temperatures (lattice parameters are almost the same).

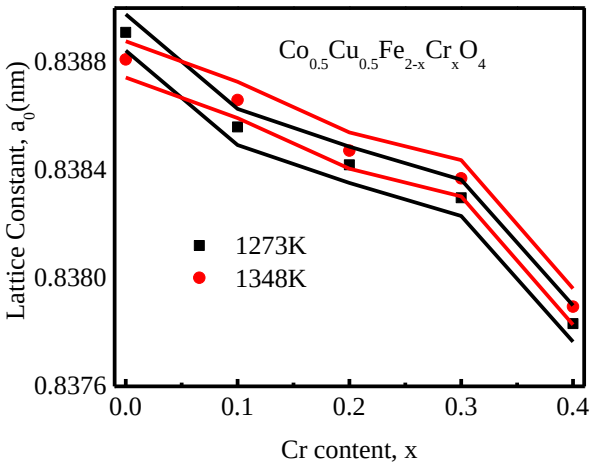

Fig. 3. Variation of lattice parameter for various $Co_{0.5}Cu_{0.5}Fe_{2-x}Cr_xO_4$ sintered at 1273 and 1348K

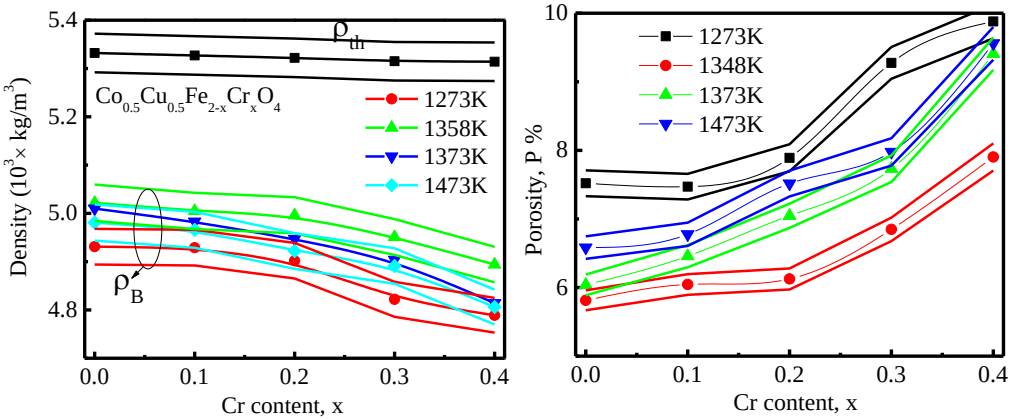

Fig. 4. ρ_{th}, ρ_B and P of $Co_{0.5}Cu_{0.5}Fe_{2-x}Cr_xO_4$ samples as a function of Cr content at different T_s

Fig. 4 denotes the ρ_{th} and ρ_B vs Cr content for various $Co_{0.5}Cu_{0.5}Fe_{2-x}Cr_xO_4$ samples at different T_s. Table 1 presents the values of 'a', ρ_{th}, ρ_B and P. The ρ_{th} is greater than that of ρ_B because the bulk samples might have some pores that emerged and were created during the sintering or sample preparation procedures. [11-12]. On the other hand, ρ_{th} does not involve any defects as it allows measurement of precise unit cell dimensions and unit cell volume and number of unit cell atoms [12]. A decreasing trend of ρ_B is found with rising Cr content because the Fe has a larger atomic mass than Cr. Fig. 4 shows that the ρ_B rises and P decreases with T_s up to 1348K, and then they follow the opposite trend with increasing T_s. At higher T_s the ρ_B decreases because the discontinuous grain growth increases. Similar results have been previously reported for NiZn ferrites [13]. P often comes from intergranular and intragranular sources depending on whether the pores are at the edges of the grains or within them.

Table 1 : The lattice constant, density, porosity, average grain size, real part of initial permeability, and relative quality factor of $Co_{0.5}Cu_{0.5}Fe_{2-x}Cr_xO_4$ sintered at various sintering temperatures in air for 5 hrs.

x	T_s (K)	a_0 (nm)	ρ_{th} ($\times10^3$kg/m^3)	ρ_B ($\times10^3$kg/m^3)	P (%)	D (μm)	μ at 16 MHz	Q
0.0	1273	0.8389	5.332	4.93	7.52	3.12	20	550
	1348			5.02	5.82	6.82	24	830
	1373			5.01	6.04	278	21	510
	1473			4.98	6.58	430	20	500
0.1	1273	0.8387	5.327	4.93	7.67	3.61	21	580
	1348			5.01	6.05	3.91	30	1200
	1373			4.98	6.46	334	22	600
	1473			4.97	6.78	466	21	500
0.2	1273	0.8384	5.322	4.90	7.89	3.93	26	780
	1348			5.00	6.13	2.47	30	1300
	1373			4.95	7.05	417	24	620
	1473			4.92	7.52	600	23	600
0.3	1273	0.8383	5.315	4.82	9.28	2.40	25	630
	1348			4.95	6.85	1.20	27	1000
	1373			4.91	7.73	378	22	580
	1473			4.89	7.98	556	21	550
0.4	1273	0.8378	5.314	4.79	9.88	1.88	19	500
	1348			4.90	7.90	1.00	21	760
	1373			4.85	7.40	298	20	580
	1473			4.81	9.56	417	19	560

Therefore, porosity can be written as

$$P = P_{intra}+P_{inter}$$

The ρ_B and P are influenced by the Ts. This can be interpreted in the following ways [14]:

i) During Ts, the force generated from the thermal energy promotes grain boundary growth over the pores resulting in reduced pore volume and thickening of the material.

ii) An excessively high grain growth rate causes the pores to become stuck inside the grain when they fall behind the fast-moving grain boundary [14]. It is practically impossible to eliminate. This persistent grain growth increases with temperature.

3.2 Microstructures

The microstructures of $Co_{0.5}Cu_{0.5}Fe_{2-x}Cr_xO_4$ at different T_ss are revealed in Figs. 5 and 6. Up to x=0.2, D for various $Co_{0.5}Cu_{0.5}Fe_{2-x}Cr_xO_4$ samples is found to increase with Cr and, after that, drops. During low T_s = 1357 K, Cu probably promotes sintering and coalesces grain development [15]. As a result, D rises as the Cr content increases to x=0.2. D drops as the Cr rises to x>0.2 because Cr has a greater melting temperature than Fe and Cu. Bhandare *et al*. reported that Cu substitution enhances grain growth [16]. T_s has a significant effect on the microstructure of this series. It has also been explored that D increases in $Co_{0.5}Cu_{0.5}Fe_{2-x}Cr_xO_4$ with increasing T_s due to developing homogeneous grain development [13]. The D values for different samples at diverse T_s are displayed in Table 1. The microstructures of $Co_{0.5}Cu_{0.5}Fe_{2-x}Cr_xO_4$ at T_s=1373K are shown in Fig.6. A large D is obtained for each sample, which confirms the textured structure.

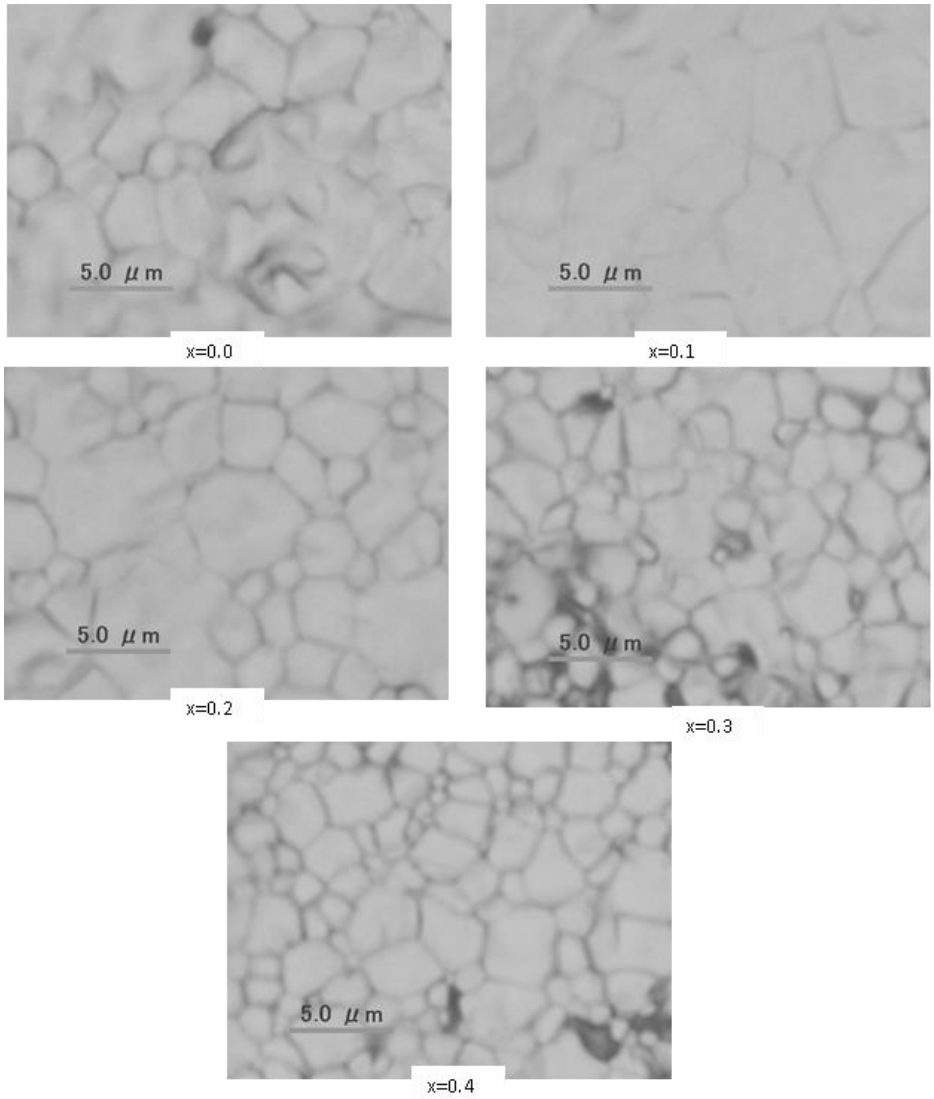

Fig. 5. The optical micrographs of $Co_{0.5}Cu_{0.5}Fe_{2-x}Cr_xO_4$ sintered at 1273K

3.3 Complex initial permeability

The room temperature frequency dependent μ_i' and μ_i'' are illustrated in Fig.7. For Cr-doped $Co_{0.5}Cu_{0.5}Fe_{2-x}Cr_xO_4$ the μ_i' was performed at four different T_ss. The μ_i'follows the same trend as D with increasing Cr for various $Co_{0.5}Cu_{0.5}Fe_{2-x}Cr_xO_4$. Table 1 shows the μ_i' values for various $Co_{0.5}Cu_{0.5}Fe_{2-x}Cr_xO_4$. The dispersion of permeability μ_i' as shown in the figure remains steady up to the entire frequency range of 120 MHz. This contribution results from domain wall motion and/or rotation [17, 18]. The μ_i'leads to the following expression:[19]

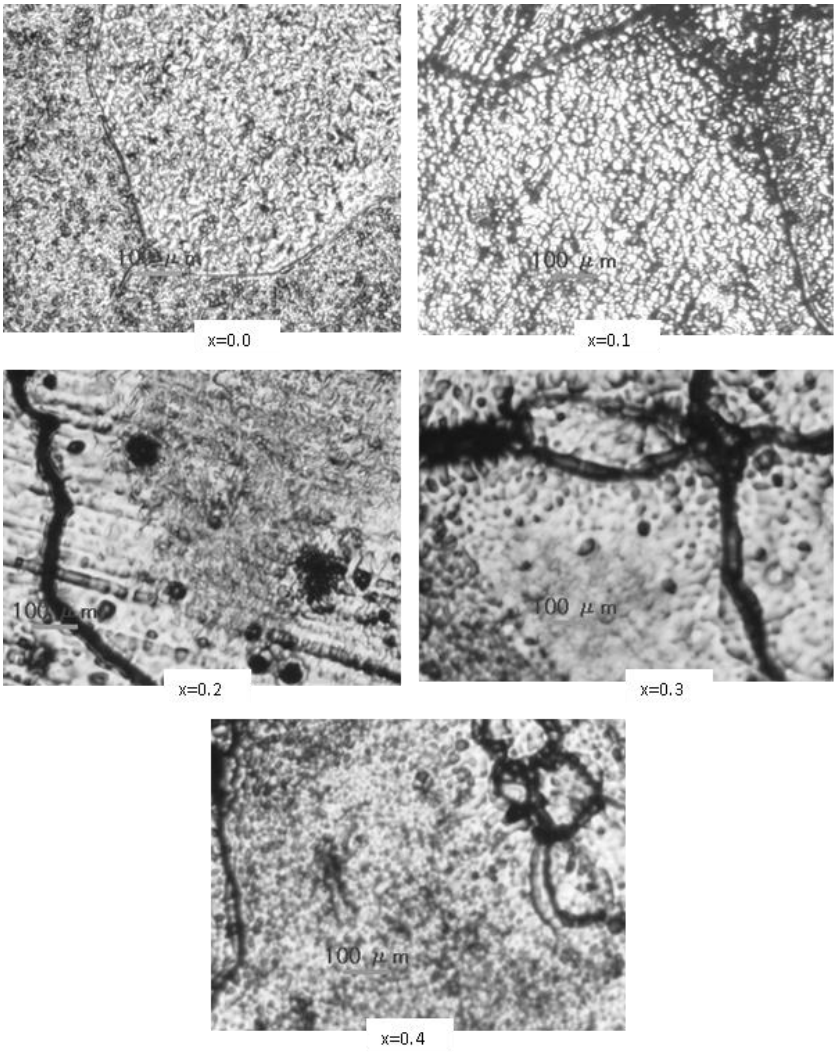

Fig.6. The optical micrograph of $Co_{0.5}Cu_{0.5}Fe_{2-x}Cr_xO_4$ sintered at 1373K

$$\mu_i^{/} \approx \frac{3\mu_0 M_s^2 D}{16\gamma_w},$$

where the free space permeability and the domain wall energy are μ_0 and γ_w, respectively. Here μ_i' varies linearly with D. Our experimental results agree with this model. A linear connection between μ_i' and D can be easily deduced from Fig. 8. It is found that the maximum values of μ_i' and ρ_B are 30 and 5.01, respectively at 1348 K. The μ_i' depends on various factors such as microstructure, porosity, density, domain wall motion, etc. The value of μ_i' may be low because imperfections (pores, cracks) typically prevent the movement of the domain wall [18].

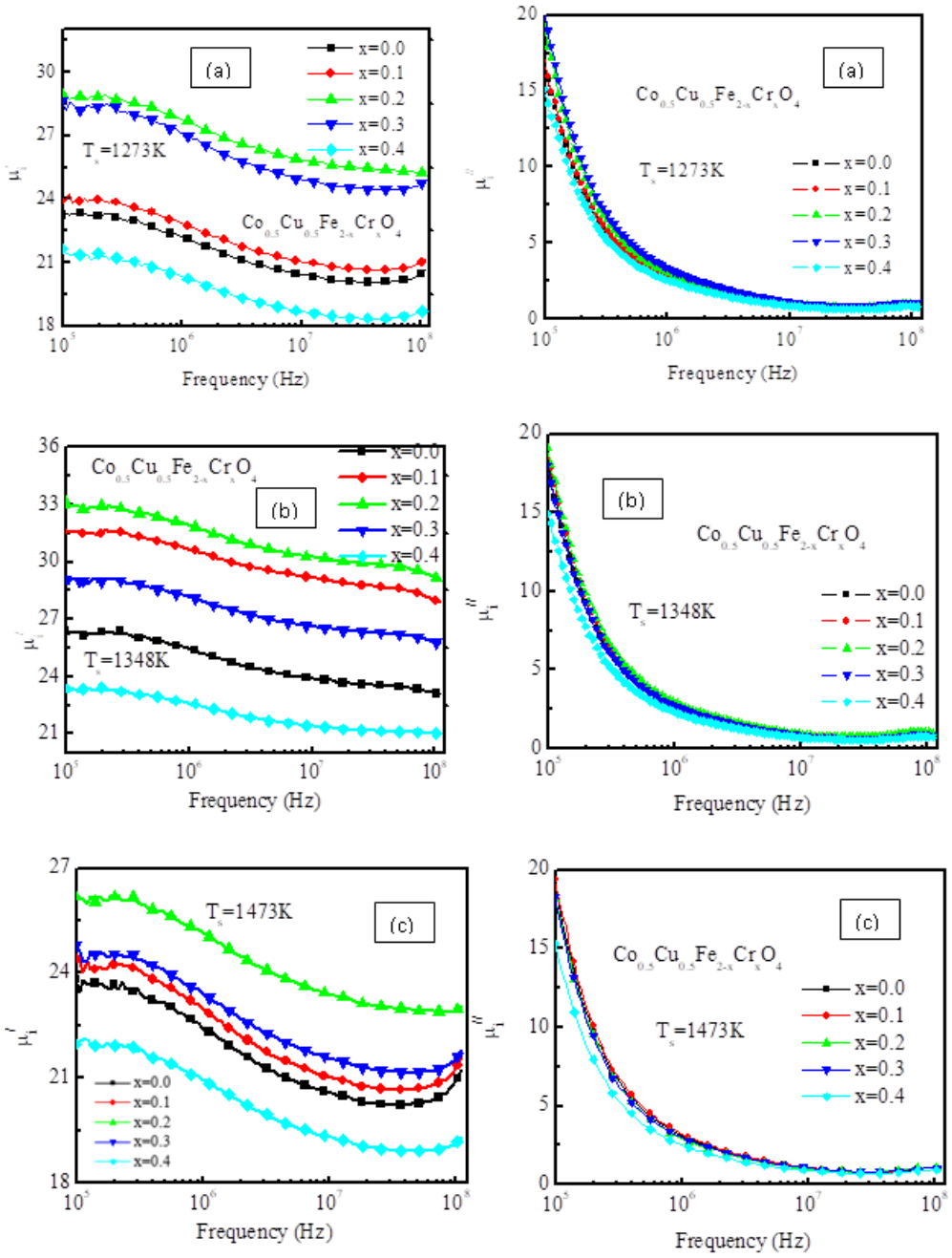

Fig. 7. The frequency dependent complex permeability for various $Co_{0.5}Cu_{0.5}Fe_{2-x}Cr_xO_4$ sintered at (a) 1273, (b) 1348 and (c) 1473K

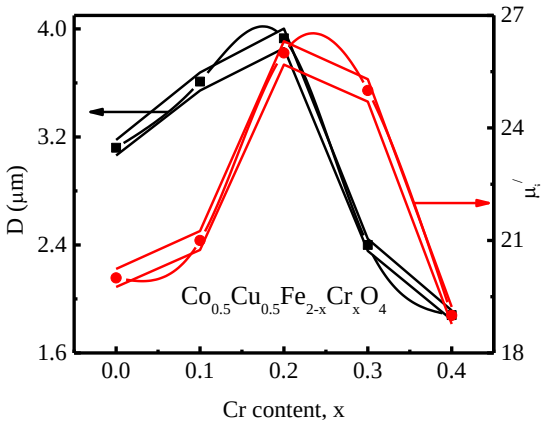

Fig. 8. The D and μ_i' as a function of Cr content for various $Co_{0.5}Cu_{0.5}Fe_{2-x}Cr_xO_4$ sintered at 1273K

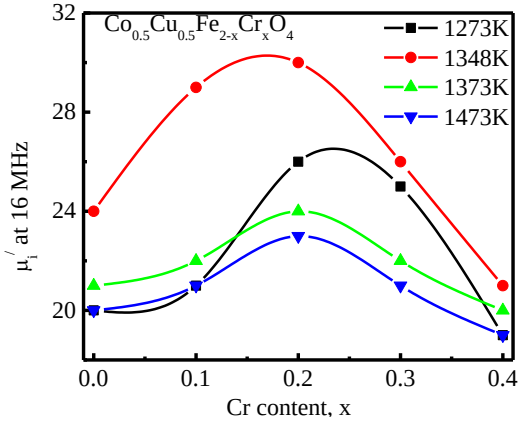

Fig. 9. The μ_i' for various $Co_{0.5}Cu_{0.5}Fe_{2-x}Cr_xO_4$ as a function of Cr sintered at 1273, 1348, 1473 and 1473K

Fig. 9 shows the μ_i'at 16MHz against Cr content for various $Co_{0.5}Cu_{0.5}Fe_{2-x}Cr_xO_4$ at different T_ss. It is revealed that μ_i' starts to increase and reaches its optimum value up to 1348K due to the evolution of grain and reduction of porosity [14, 15] and then the μ_i'starts to decrease due to discontinuous grain growth. Therefore μ_i' is controlled by both ρ_B and microstructure, which depends on T_s [14, 15]. Similar behavior was previously reported by Zehani et al. [20].

The Changes in Q_{max} for different $Co_{0.5}Cu_{0.5}Fe_{2-x}Cr_xO_4$ for different T_s with Cr content are expressed in Fig. 10. Q follows the same trend as revealed in the case of μ_i'. The loss is attributed to lattice defects and is induced by the delay of domain wall movement relative to the applied field. The loss increases with Ts due to introducing certain lattice defects that enhance the magnetic loss [21]. The highest Q_{max} (1300) is found for $Co_{0.5}Cu_{0.5}Fe_{1.8}Cr_{0.2}O_4$ sintered at 1348K.

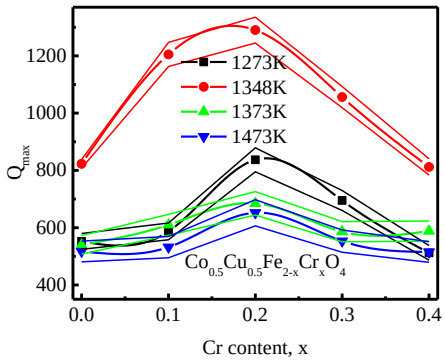

Fig. 10. The Q_{max} for various $Co_{0.5}Cu_{0.5}Fe_{2-x}Cr_xO_4$ as a function of Cr sintered at 1273, 1348, 1473 and 1473K

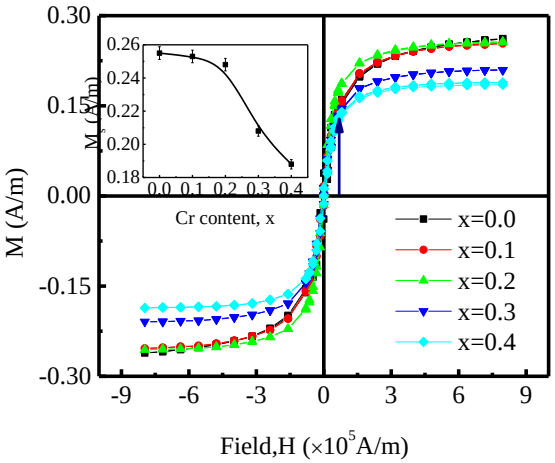

Fig. 11. Room temperature M-H loops for various $Co_{0.5}Cu_{0.5}Fe_{2-x}Cr_xO_4$ sintered at 1273K

Table 2: The cation distribution, coercivity, remanent magnetization, room temperature saturation magnetization, and magnetic moment of various $Co_{0.5}Cu_{0.5}Fe_{2-x}Cr_xO_4$ sintered at 1273K in air for 5hrs.

x	Cation distribution	H_c (10^3×A/m) at 10K	M_r (A/m) at 10K	M_s at 7.17×10^5 (A/m)	n_B (μ_B) (theory)	n_B (μ_B) (expt)	T_N (K)
0.0	$(Cu^{2+}_{0.1}Fe^{3+}_{0.9})[Co^{2+}_{0.5}Cu^{2+}_{0.4}Fe^{3+}_{1.1}]O_4$	134	0.159	0.255	2.8	2.25	826
0.1	$(Cu^{2+}_{0.1}Fe^{3+}_{0.9})[Co^{2+}_{0.5}Cu^{2+}_{0.4}Cr^{3+}_{0.1}Fe^{3+}_{1.0}]O_4$	67	0.178	0.253	2.6	2.16	803
0.2	$(Cu^{2+}_{0.1}Fe^{3+}_{0.9})[Co^{2+}_{0.5}Cu^{2+}_{0.4}Cr^{3+}_{0.2}Fe^{3+}_{0.9}]O_4$	59	0.221	0.251	2.4	2.12	663
0.3	$(Cu^{2+}_{0.1}Fe^{3+}_{0.9})[Co^{2+}_{0.5}Cu^{2+}_{0.4}Cr^{3+}_{0.3}Fe^{3+}_{0.8}]O_4$	80	0.186	0.208	2.2	1.79	
0.4	$(Cu^{2+}_{0.1}Fe^{3+}_{0.9})[Co^{2+}_{0.5}Cu^{2+}_{0.4}Cr^{3+}_{0.4}Fe^{3+}_{0.7}]O_4$	89	0.183	0.188	2.0	1.62	638

3.4 M-H Loop and Saturation Magnetization

Fig.11 demonstrates the room temperature H–M loops of the Cr-substituted $Co_{0.5}Cu_{0.5}Fe_{2-x}Cr_xO_4$ at T_s=1273K and the inset Fig. represents the variation of M with variation of Cr. It is noticed that the magnetization rises linearly for all samples with rising applied fields and reaches saturation at higher fields. The investigated samples are ferromagnetic up to low field (64 kA/m). The values of M_s determined from the figure for each sample are presented in Table 2.

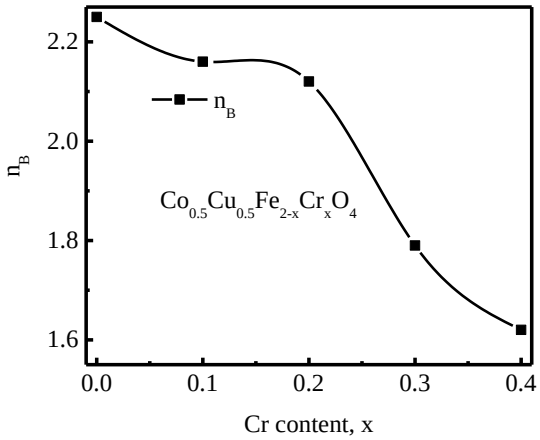

Fig. 12. The variation of n_B in terms if μ_B as function of Cr content for various $Co_{0.5}Cu_{0.5}Fe_{2-x}Cr_xO_4$ sintered at 1273K

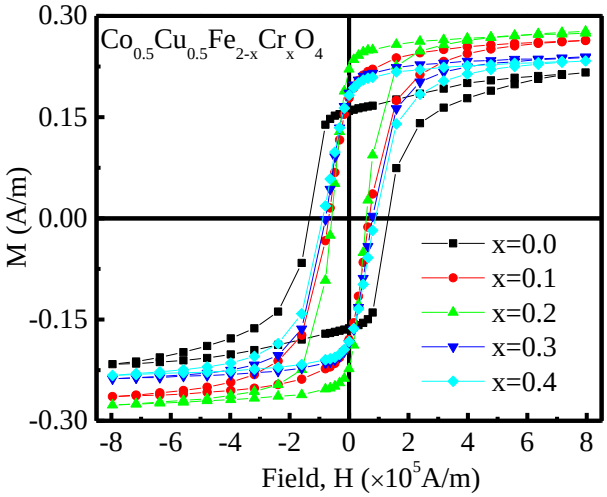

Fig. 13. M-H loops at 10K for various $Co_{0.5}Cu_{0.5}Fe_{2-x}Cr_xO_4$ sintered at 1273K

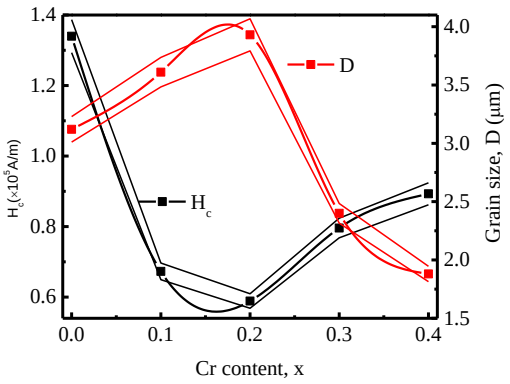

Fig. 14. The variation of H_c and D as function of Cr content for various $Co_{0.5}Cu_{0.5}Fe_{2-x}Cr_xO_4$ sintered at 1273K

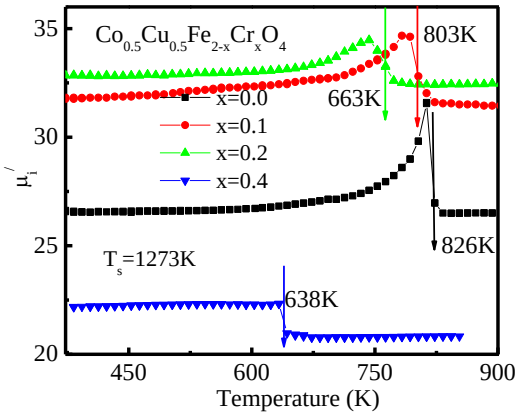

Fig. 15. The normalized temperature dependent $\mu_i^{/}$ as a function of Cr content for various $Co_{0.5}Cu_{0.5}Fe_{2-x}Cr_xO_4$ sintered at 1273K

The reduction of M_s with Cr content depends on the distribution of Co^{+2}, Cr^{+3}, Cu^{+2} and Fe^{+3} ions and A-B interactions. Based on the reports of Verma et al.[22], Lakhani et. al [23] and Lee et.al [24], the cations of this series may be distributed in the following way:

$$(Cu_{0.1}^{2+}Fe_{0.9}^{3+})[Co_{0.5}^{2+}Cu_{0.4}^{2+}Cr_x^{3+}Fe_{1.1-x}^{3+}]O_4,$$

where the parenthesis represents A-site, and the square bracket represents B-site. The A–B interaction weakens because (i) the preferred location of Cr^{3+} is at the B-site [5, 22, 24] , (ii) Fe is replaced by Cr, which is linked to the A-site through O, and (iii) Cr's ($3\mu_B$) magnetic moment is less than Fe's ($5\mu_B$). Fig.12 illustrates the variation of the magnitude of Bohr magneton, n_B with Cr. The n_Bs for the samples are shown in Table 2. The n_B falls, because M_s reduces as the Cr content rises. Fig.13 shows that M-H loop at 10K for various $Co_{0.5}Cu_{0.5}Fe_{2-x}Cr_xO_4$ sintered at 1273K. Table 2 displays the H_C and remanence magnetization (M_r)) values of this series as determined by the M-H

loop at 10K. The H_c of these compositions decreases as Cr increases up to 0.2 and then increases, as seen in Figure 14. We observed that H_c is inversely proportional to the D. The decreasing H_c may be explained by the following way.

Dehlinger et al. reported that the relationship between Hc and D is inverse [25]. Verma et al. reported that H_C decreases as T_s and D increase [26] . Our results are in agreement with the published articles mentioned above. It is observed from Figs. 11 and 13 that H_c and M_s of 10K are more significant than that of 300K.

The larger H_C and M_s are observed at 10K compared to room temperature. These are due to increased magnetic anisotropy at low temperatures [25, 27]. Samples of various $Co_{0.5}Cu_{0.5}Fe_{2-x}Cr_xO_4$ are magnetically harder at 10 K due to spin freezing [28].

3.5 Néel temperatures

Fig. 15 demonstrates the normalized $\mu_i^/$ at constant 100 kHz with temperature variation for various $Co_{0.5}Cu_{0.5}Fe_{2-x}Cr_xO_4$ samples. The $\mu_i^/$ rises gradually with temperature, comes to its highest point and then decreases suddenly at a specific temperature (referred as T_N) with a tailing effect. Thermal energy in T_N destroys the ferromagnetic order of the ferrite sample and changes it to a paramagnetic order. A similar effect has been observed by Arulmurugan et al.[29]. The rapid decrease of $\mu_i^/$ at T_N confirms the homogeneity of the various Co0.5Cu0.5Fe2-xCrxO4 as reported by Jehani et al.[30]. The sharp rise in $\mu_i^/$ just below T_N can be explained in the following way:

$$\mu_i^/ = \frac{M_S^2 D}{K_1},$$

where K_1 is the crystal anisotropy.

As temperature rises, rises as well, goes to infinity just below T_N, and enters the paramagnetic order at T_N because K_1 declines more quickly than M_s [14, 31]. The T_N decreases as the amount of Cr substitution increases in $Co_{0.5}Cu_{0.5}Fe_{2-x}Cr_xO_4$. as shown in Table 2. This is reduced due to the weakening of the A-B exchanged energy, which has already been explained in section 3.4.

4. CONCLUSIONS

Cr-substituted polycrystalline $Co_{0.5}Cu_{0.5}Fe_{2-x}Cr_xO_4$ ferrites have been investigated. The unique phase spinel structure of each sample was confirmed from XRD studies. The Textured crystal structure of $Co_{0.5}Cu_{0.5}Fe_{2-x}Cr_xO_4$ observed at 1373K is confirmed by the preferred orientation of XRD analysis and the large average grain size of microstructural analysis. D increases with increasing Cr content up to 0.2, then decreases with increasing Cr, whereas coercivity follows the opposite trend. This occurred because Cu ions promote grain growth during the sintering process for a low concentration of Cr. In $Co_{0.5}Cu_{0.5}Fe_{2-x}Cr_xO_4$, the $\mu_i^/$ increases to x=.2 under the influence of Cr concentration. It depends on the grain growth and the coercivity. The M_s and T_N decrease when Cr is substituted for the Fe in $Co_{0.5}Cu_{0.5}Fe_{2-x}Cr_xO_4$ because the A-B super-exchange interaction weakens with increasing Cr. Due to the high T_N (T_N=826K for $Co_{0.5}Cu_{0.5}Fe_2O_4$ and T_N=638K for $Co_{0.5}Cu_{0.5}Fe_{1.6}Cr_{0.4}O_4$) these may be conducted above room temperature. The samples sintered at 1348K show a good compromise in terms of high-frequency response permeability, RQ, and moderate T_N. So, the investigated $Co_{0.5}Cu_{0.5}Fe_{2-x}Cr_xO_4$ ferrites may be good candidates for preparing multilayer chip inductors.

REFERENCES

[1] A. Lucas, R. Lebourgeois, F. Mazaleyrat, E. Laboure, J. Magn. Magn. Mater. 323(2011)735–739
[2] S. J. Lee, C. C. H. Lo, P. N. Matlage, S. H. Song, Y. Melikhov, J. E. Snyder, and D. C. Jiles, J. Appl. Phys. 102,073910 (2007)
[3] Ph. Tailhades, C. Villette, A. Rousset, Paul Sabatier, G. U. Kulkarni, K. R. Kannan, C. N. R. Rao, M. Lenglet, J. Solid State Chemistry, 141, 56-63 (1998)
[4] Hua Su, Huaiwu Zhang, Xiaoli Tang, Yulan Jing, and Baoyuan Liu, IEEE Trans. Magn. 452050-2052 (2009)
[5] S. T. Alone, Sagar E. Shirsatha, R. H. Kadamb, K. M. Jadhava, J. Alloys Compd.509(2011) 5055–5060
[6] M. R. Bhandarea, H. V. Jamadarb, A. T. Pathanb, B. K. Chouguleb, A. M. Shaikhc, J. Alloys Compd. 509 (2011) L113–L118
[7] M. Penchal Reddy, W. Madhuri, M. Venkata Ramana, N. Ramamanohar Reddy, K. V. SivaKumar, V. R. K. Murthy, K. Siva Kumar, R. Ramakrishna Reddy, J. Mang. Mang. Mater. 322 (2010) 2819–2823
[8] Panda R, Muduli R, Jayarao G, Sanyal D, Behera D, J. Alloys Comp. 669, 19- 28 (2016)
[9] D. Ravinder, K. Sathi Reddy, P. Mahesh, T. Bhaskar Rao, Y. C. Venudhar, J. Alloys Compd. 370 (2004) L17–L22
[10] Aria Yang, X. Zuo, L. Chen, Z. Chen, C. Vittoria, and V. G. Harris, J. Appl. Phys. 97, 10G107 (2005)
[11] Sagar E. Shirsath, Santosh S. Jadhav, B. G. Toksha, S. M. Patange, and K. M. Jadhav, J. Appl. Phys. 110, 013914 (2011)
[12] B. D. Cullity, S. R Stock, Prentice Hall, 2001
[13] M. Siva Ram Prasad, B. B. V. S. V. Prasad, B. Rajesh, K. H. Rao, K. V. Ramesh, J. Magn. Magn. Mater.323 (2011) 2115–2121
[14] Raul Valenzuela, Cambridge University Press,(1994)
[15] J. Smit, and H. Wijn, Ferrites, Wiley, (Philips Technical Library, Eindhoven, Netherland), Chapter 8, 1959.
[16] M. R. Bhandare, H. V. Jamadar, A. T. Pathan, B. K. Chougule, A. M. Shaikh, J. Alloys and Compd. 509 (2011) L113–L118
[17] G. T. Rado, R. W. Wright, W. H. Emerson, Phys. Rev. **80** (1950) 273.
[18] Alex Goldman, Springer Publishing, 2006.
[19] A, Globus, P. Duplex and Guyot, IEE Trans. Magn. 7 (1971) 617-622.
[20] K. Zehani, F. Mazaleyrat, V. Loyau, and E. Laboure, J. Appl. Phys. 109, 07A504 (2011)
[21] Amarendra K. Singh, T. C. Goel, and R.G. Mendirattaa O. P. Thakur and Chandra Prakash, J. Appl. Phys. 92 (2002) 3872-3876.
[22] M. Chaitanya Varma, S. Bharadwaj, K. Vijaya Babu, J. Physica B: Condensed Matter, 556, 175-182 (2019)
[23] V. K. Lakhani, Bangchuan Zhao, Lan Wang, U. N. Trivedi, K. B. Modi, J. Alloys. Compd. 509 (2011) 4861–4867
[24] S. J. Lee and C. C. H. Lo, P. N. Matlage and S. H. Song, Y. Melikhov, J. E. Snyder, and D. C. Jiles , J. Appl. Phys. 102, 073910 (2007)
[25] A. S. Dehlinger, M. Le Berre, B. Canut, J. P. Chatelon, D. Albertini, S. Perrot, D. Givord, J. J. Rousseau, J. Magn. Magn. Mater. 322 (2010) 3293– 3297
[26] A. Verma, T. C. Goel, Mendiratta and P. Kishan, J. Magn. Magn. Mater. 208 (2000) 13-19
[27] K. Maaz, A. Mumtaz, S. K. Hasanain, M. F. Bertino, J. Magn. Magn. Mater. 322 (2010) 2199–2202.
[28] J. Z. Msomi, H. M. I. Abdallah, T. Moyo, A. Lancok, J. Magn. Magn. Mater. 323 (2011) 471–474.
[29] Arulmurugan, R., Jeyadevan, B., Vaidyanathan, G. and Sendhilnathan, S., J. Magn. Magn. Mater., 288: 470–477,2005.
[30] S. A. Ghodake, U. R. ghodake, S. R. Sawant, S.SSuryavanshi, P. PBakare, J. Magn. Magn. Mater. 305 (2006) 110–119
[31] D. N. Bhosale, N. D. Choudhari, S. R. Sawant, P. P. Bakare, J. Magn. Magn. Mater. **173** (1997) 51.
[32] L. Néel, Acad. Sci., Paris, C. R. 230, 375 (1950)